Title

Long-term neurocognitive benefits of FLASH radiotherapy driven by reduced reactive oxygen species

Journal

Proceedings of the National Academy of Sciences of the United States of America, 116(22)

ISSN

0027-8424

Authors

Montay-Gruel, Pierre
Acharya, Munjal M
Petersson, Kristoffer
et al.

Publication Date

2019-05-28

DOI

10.1073/pnas.1901777116

Peer reviewed

Long-term neurocognitive benefits of FLASH radiotherapy driven by reduced reactive oxygen species

Pierre Montay-Gruel[a,b,1], Munjal M. Acharya[c,1], Kristoffer Petersson[a,b,d], Leila Alikhani[c], Chakradhar Yakkala[a,b], Barrett D. Allen[c], Jonathan Ollivier[a,b], Benoit Petit[a,b], Patrik Gonçalves Jorge[a,b,d], Amber R. Syage[c], Thuan A. Nguyen[c], Al Anoud D. Baddour[c], Celine Lu[c], Paramvir Singh[c], Raphael Moeckli[d], François Bochud[d], Jean-François Germond[d], Pascal Froidevaux[d], Claude Bailat[d], Jean Bourhis[a,b], Marie-Catherine Vozenin[a,b,2,3], and Charles L. Limoli[c,2,3]

[a]Laboratory of Radiation Oncology, Lausanne University Hospital, University of Lausanne, Lausanne VD-1011, Switzerland; [b]Department of Radiation Oncology, Lausanne University Hospital, University of Lausanne, Lausanne VD-1011, Switzerland; [c]Department of Radiation Oncology, University of California, Irvine, CA 92697-2695; and [d]Institute of Radiation Physics, Lausanne University Hospital, University of Lausanne, Lausanne VD-1011, Switzerland

Edited by James E. Cleaver, University of California, San Francisco, CA, and approved April 18, 2019 (received for review February 12, 2019)

Here, we highlight the potential translational benefits of delivering FLASH radiotherapy using ultra-high dose rates (>100 Gy·s^{-1}). Compared with conventional dose-rate (CONV; 0.07–0.1 Gy·s^{-1}) modalities, we showed that FLASH did not cause radiation-induced deficits in learning and memory in mice. Moreover, 6 months after exposure, CONV caused permanent alterations in neurocognitive end points, whereas FLASH did not induce behaviors characteristic of anxiety and depression and did not impair extinction memory. Mechanistic investigations showed that increasing the oxygen tension in the brain through carbogen breathing reversed the neuroprotective effects of FLASH, while radiochemical studies confirmed that FLASH produced lower levels of the toxic reactive oxygen species hydrogen peroxide. In addition, FLASH did not induce neuroinflammation, a process described as oxidative stress-dependent, and was also associated with a marked preservation of neuronal morphology and dendritic spine density. The remarkable normal tissue sparing afforded by FLASH may someday provide heretofore unrealized opportunities for dose escalation to the tumor bed, capabilities that promise to hasten the translation of this groundbreaking irradiation modality into clinical practice.

ultra-high dose-rate irradiation | cognitive dysfunction | neuronal morphology | neuroinflammation | reactive oxygen species

Radiation therapy (RT) remains an essential part of cancer treatment, and, today, the benefit of RT would increase dramatically if normal tissues surrounding the tumor could tolerate higher doses of radiation (1–3). In the last decade, major advances in high-precision treatment delivery and multimodal imaging have improved tolerance to RT (4), but the selective protection of normal tissue remains a significant clinical challenge and the radiation-induced toxicities still adversely impact the patient's quality of life. This latter fact largely remains an unmet medical need, and points to the urgency of developing improved RT modalities for combating those cancers refractory to treatment.

This issue is especially critical for those afflicted with brain tumors, including glioblastoma multiforme (GBM), for which standard treatment consists of surgical resection followed by RT and concomitant chemotherapy (temozolomide). Typical radiotherapeutic protocols for GBM induce neurocognitive complications, including impairments in learning and memory, attention, and executive function and a variety of mood disorders (5–8). A breadth of past work from our laboratories has linked adverse neurocognitive outcomes following cranial irradiation to a range of neuropathologies, including reductions in dendritic complexity and spine density (9–12), reductions in microvascular density (13–15), reduced myelination and synapse density, and increased neuroinflammation (16, 17). These changes are persistent and problematic in the conventionally irradiated brain and have prompted efforts to more fully develop a truly innovative approach to RT, where we have conceptualized and implemented a modality of irradiation named FLASH radiotherapy (FLASH-RT) (18, 19). Cognitive sparing was demonstrated when single doses of 10 Gy were delivered at dose rates exceeding 100 Gy·s^{-1}, with an apparent threshold when dose rates fell below ~30 Gy·s^{-1} (19). While existing data indicate that FLASH-RT does not induce neurocognitive impairment, comprehensive studies investigating the mechanistic basis of the beneficial "FLASH effect" remained to be undertaken.

Using healthy mouse models, we undertook direct comparisons between FLASH-RT and conventional dose-rate (CONV) irradiation modalities that were facilitated throughout this study by performing all experiments under isodose conditions. We found that FLASH-irradiated mice did not exhibit neurocognitive decline, and were spared a host of associated pathologies. Further mechanistic experimentation explored the physicochemical basis of the FLASH effect (20) through the modulation of oxygen

Significance

Ultra-high dose-rate (≥100 Gy·s^{-1}) irradiation, termed FLASH radiotherapy, affords some remarkable (if not unexpected) normal tissue sparing in the irradiated brain when compared with conventional dose rates (0.07–0.1 Gy·s^{-1}) used in clinical practice. Radiation-induced neurocognitive deficits, persistent neuroinflammation, and the structural degradation of mature neurons, typical of conventional dose-rate exposures, were resolved significantly in a preclinical mouse model exposed to FLASH radiotherapy. These benefits persisted over a 6-mon postirradiation interval and were caused, in part, by a mechanism involving reduced reactive oxygen species. Since normal tissue injury during and following radiotherapy dictates the maximum tolerated dose, the capability to ameliorate these adverse side effects holds significant promise for improving therapeutic outcome for cancer survivors worldwide.

Author contributions: P.M.-G., M.M.A., K.P., M.-C.V., and C.L.L. designed research; P.M.-G., M.M.A., L.A., C.Y., B.D.A., J.O., B.P., P.G.J., A.R.S., T.A.N., A.A.D.B., C.L., P.S., R.M., F.B., P.F., and C.B. performed research; P.M.-G., M.M.A., K.P., J.-F.G., C.B., J.B., M.-C.V., and C.L.L. analyzed data; and P.M.-G., M.M.A., M.-C.V., and C.L.L. wrote the paper.

The authors declare no conflict of interest.

This article is a PNAS Direct Submission.

[1]P.M.-G. and M.M.A. contributed equally to this work.

[2]M.-C.V., and C.L.L. contributed equally to this work.

[3]To whom correspondence may be addressed. Email: marie-catherine.vozenin@chuv.ch or climoli@uci.edu.

This article contains supporting information online at www.pnas.org/lookup/suppl/doi:10.1073/pnas.1901777116/-/DCSupplemental.

concentration in the brain. We found that by doubling the oxygen content through carbogen breathing, the neurocognitive benefits of FLASH-RT found after normoxic exposure conditions were eliminated. These data point to the critical importance of local oxygen levels, and suggest a rapid radiation-induced depletion of O_2 that elicits tissue hypoxia, thereby pointing to a fundamental and initial physicochemical mechanism for the FLASH effect. In addition, we identified subsequent mechanisms of neuroprotection in the FLASH-irradiated brain, thereby promoting the translational potential of this promising modality for minimizing normal tissue toxicity following the treatment of brain cancer.

Results

FLASH-RT Does Not Induce Cognitive Dysfunction. We investigated the impact of FLASH-RT on short-term and longer term neurocognitive sequelae typically found after CONV treatments. Cognitive studies were conducted in tumor-free animals so that behavioral data could be collected and evaluated under carefully controlled conditions and in the absence of confounding disease that would otherwise cause premature death of the animal before long-term analyses.

Thus, studies were initiated 1 mo after irradiation on animals subjected to a series of spontaneous exploration tasks known to interrogate hippocampal and frontal cortical learning and memory. Animals exposed to the cranial 10-Gy FLASH irradiation and subjected to the novel object recognition (NOR) task (Fig. 1*A*) were statistically indistinguishable from controls, whereas the 10-Gy CONV–irradiated cohort exhibited a reduction in their discrimination index (DI). Significantly, no loss of performance on this task was shown up to 12 Gy delivered as FLASH-RT, but the FLASH effect was finally lost in cohorts exposed to 14 Gy, where animals exhibited an impaired NOR performance (reduced DI) comparable to the CONV cohort (*SI Appendix*, Fig. S1). Following NOR testing, mice were habituated and tested on the object in place (OIP) and temporal order (TO) tasks (Fig. 1 *B* and *C*). Similarly, the two tests showed that the 10-Gy FLASH cohort was statistically indistinguishable from controls, whereas the CONV cohort showed a drop in cognitive function. Importantly, mice from all cohorts subjected to spontaneous exploration tasks exhibited normal motor function and exploration.

Longer term studies (6 mo post-RT) were then conducted to determine the persistence of the neuroprotective FLASH effect. To analyze whether irradiated mice exhibited differences in behavioral characteristics indicative of anxiety and/or depression, animals were subjected to an elevated plus maze (EPM) test and a light-dark box (LDB) test to quantify anxiety behavior, along with a forced swim test (FST) used to quantify depression behavior. Cohorts subjected to 10-Gy FLASH showed reduced anxiety- and depression-like behavior compared with CONV-irradiated mice (Fig. 1 *D*–*F*). The capability of FLASH to indefinitely extend the onset and minimize the severity of persistent radiation-induced mood disorders suggests that FLASH does not trigger neurotoxic pathways.

The fact that anxiety and depression are not found after FLASH-RT suggests a possible impact on extinction memory. Therefore, mice were subjected to a rigorous protocol designed to determine whether they could unlearn the association between a tone and mild foot shock (Fig. 1*G*). Data obtained confirmed the nontoxic effects of FLASH-RT, as both control and FLASH cohorts exhibited a progressive decline in freezing behavior over extinction training. In contrast, CONV-irradiated mice showed significantly higher freezing behavior ($P < 0.05$–0.0001) (Fig. 1*G*). Animals subjected to the fear extinction test 24 h after the cessation of the extinction trials showed significant overall group differences [$F_{(2,25)} = 7.27$, $P < 0.01$] (Fig. 1*G*, *g1*). Importantly, these differences persisted, as extinction between controls and the FLASH cohort was identical, while CONV-irradiated animals remained impaired. Cognitive data collected over 6 mo following exposure provide compelling evidence for the long-term neurocognitive sparing of FLASH-RT compared with CONV irradiation.

Physicochemical Basis of the FLASH Effect: Minimizing Reactive Oxygen Species Production. To rationalize the significant neuroprotection afforded by FLASH, we postulated that delivering radiation at ultra-high dose rates could reduce the yields of reactive oxygen species (ROS) through a rapid depletion of local oxygen concentration. To test this hypothesis in vivo, we increased oxygen concentration in the brain via carbogen breathing before and during 10-Gy whole-brain irradiation (WBI) (Fig. 2*A*). Carbogen breathing, per se, had no impact on the DI (mean ± SEM) of nonirradiated mice (58.34 ± 2.63 vs. 60.11 ± 2.28; $P = 0.7990$). No significant difference in DI was observed in the carbogen- or air-breathing cohorts given CONV irradiation (14.05 ± 5.61 vs. 8.95 ± 2.29; $P = 0.2234$). Notwithstanding, a significant drop in DI was observed in the carbogen-breathing mice irradiated with FLASH-RT compared with air-breathing mice irradiated with the same irradiation modality (28.53 ± 4.27 vs. 52.99 ± 1.99; $P = 0.0079$). These striking results show that a simple doubling of the oxygen concentration in the brain during irradiation was sufficient to reverse the neurocognitive benefits of FLASH-RT. This experiment supports our initial hypothesis that the beneficial effects of FLASH-RT are, in part, dependent on local oxygen concentration and ROS production.

FLASH Irradiation Produces Less H_2O_2. To corroborate further our underlying hypothesis, we specifically tested whether a given isodose of FLASH would lead to lower levels of ROS compared with CONV irradiation. Therefore, we quantified a critical end product of water radiolysis, namely, H_2O_2, using a cell-free radiochemical assay with AmplexRed after either irradiation modality (Fig. 2*B*). An aqueous oxygen concentration of 4% was used as a mimetic of physiological oxygen tension. Interestingly, and for all doses above 10 Gy, a significantly lower concentration of H_2O_2 was observed in aqueous solutions subjected to FLASH irradiation ($P < 0.001$) compared with CONV irradiation, supporting our hypothesis that FLASH-RT reduces the production of toxic ROS.

Additional studies analyzing the clonogenic survival of irradiated cells corroborated earlier work (20, 21) and showed that FLASH doses of sufficient magnitude were radioprotective under physiological oxygen conditions. Thus, while the lower dose of 10 Gy was equitoxic (*SI Appendix*, Fig. S2 *A* and *B*), the higher FLASH dose of 20 Gy (*SI Appendix*, Fig. S2*B*) was necessary to demonstrate improved clonogenic survival compared with CONV. Moving to a more physiological model involving zebrafish embryos, ROS scavenging using amifostine (*SI Appendix*, Fig. S2*C*) and *N*-acetyl cysteine (NAC; *SI Appendix*, Fig. S2*D*) was performed during FLASH and CONV irradiations. Body length measurements 5 d postfertilization (dpf; size ± SD) revealed that CONV irradiation of 4-h postfertilization (hpf) embryos led to significant subsequent developmental alterations compared with nonirradiated animals (1,255 ± 98.8 vs. 1,650 ± 25.3; $P < 0.0001$). FLASH-irradiated embryos showed significantly fewer alterations in body length (1,349 ± 153 vs. 1,650 ± 25.3; $P < 0.0001$). Zebrafish embryos preincubated with either antioxidant were protected from CONV radiation injury (1,338 ± 111 vs. 1,255 ± 98.8; $P = 0.018$), whereas no further protection was observed in the FLASH-RT groups (1,410 ± 27.0 vs. 1,349 ± 42.2; $P = 0.2402$). Moreover, even with the amifostine treatment, reductions in body length of CONV-irradiated embryos were still more extensive than in the FLASH group without any treatment. The absence of biological impact

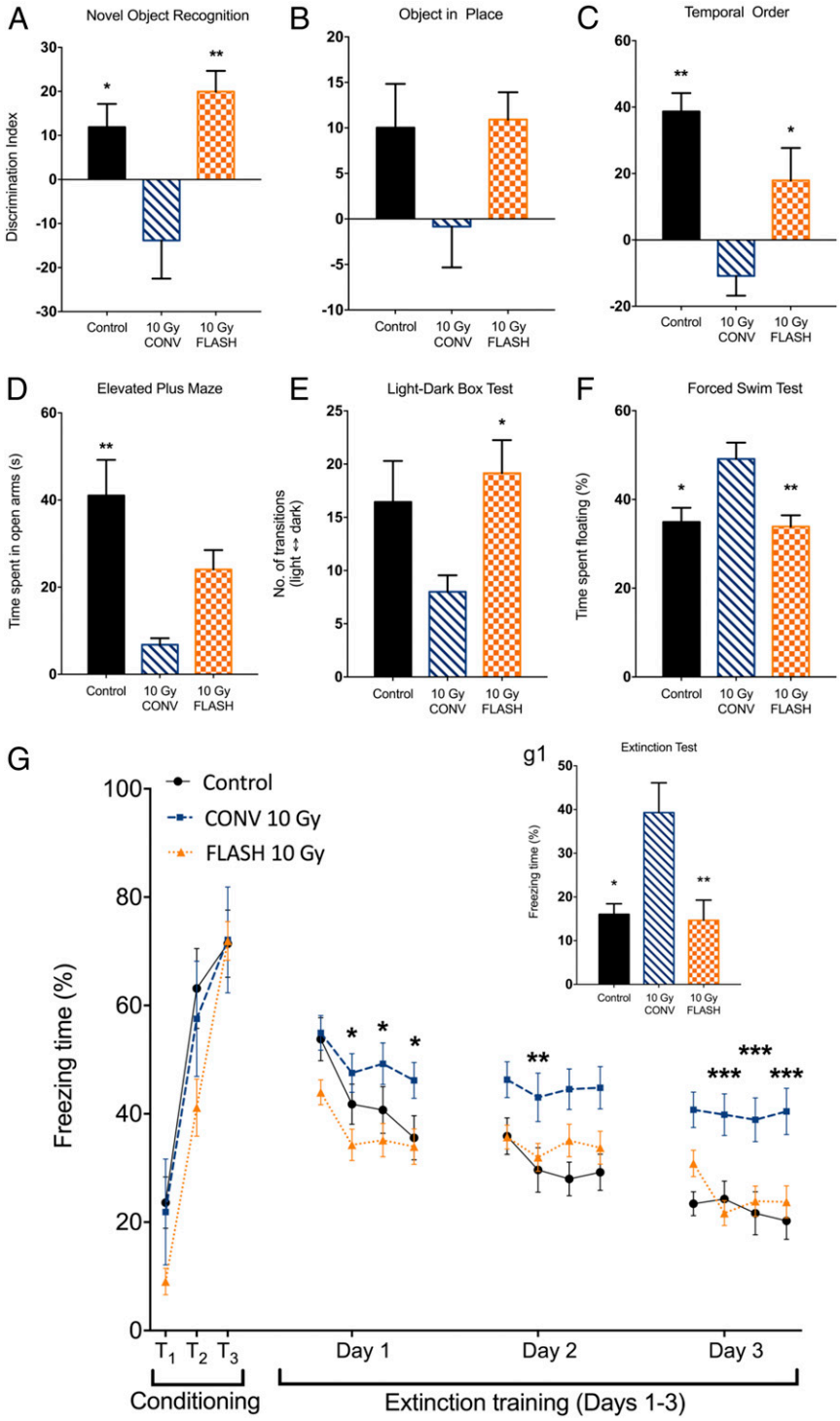

Fig. 1. FLASH-RT minimizes radiation-induced neurocognitive complications. WT mice were tested for cognitive function using the NOR (*A*), OIP (*B*), and TO (*C*) tasks. CONV irradiation (10 Gy) caused significant reductions in the DI on the NOR and TO tasks and similar trends on the OIP task compared with controls. In each instance, FLASH-RT prevented radiation-induced cognitive deficits. Mean ± SEM (n = 8–12 mice per group). P values were derived from ANOVA and the Bonferroni test. $^{*}P < 0.05$, $^{**}P < 0.01$ compared with the 10-Gy CONV group. At 6 mo post-RT, mice were subjected to the EPM test (*D*), LDB test (*E*), and FST (*F*). Mice subjected to CONV irradiation spent significantly less time in the open arms of the EPM and exhibited significantly fewer transitions between the light and dark regions of the LDB compared with controls. In contrast, FLASH cohorts showed a significant increase in the number of transitions between the light and dark compartments compared with CONV cohorts. Mice exposed to CONV irradiation spent significantly more time floating compared with either controls or the FLASH cohort. Mean ± SEM (n = 8–10 mice per group). P values were derived from ANOVA and the Bonferroni test. $^{*}P < 0.05$, $^{**}P < 0.01$ compared with the 10-Gy CONV group. (*G*) Exposure to either irradiation modality did not impair the acquisition of conditioned fear (three tone-shock pairings). All mice showed a gradual decrease in freezing behavior over the 20 extinction trials (tone only); however, the time spent freezing was significantly greater for the mice irradiated with CONV compared with controls or the FLASH cohort. (*g1*) Control and FLASH mice successfully abolished fear memory compared with the CONV group. Mean ± SEM (n = 8–10 mice per group). P values were derived from two-way repeated ANOVA followed by the Bonferroni test: $^{*}P < 0.05$, $^{**}P < 0.01$, $^{***}P < 0.001$.

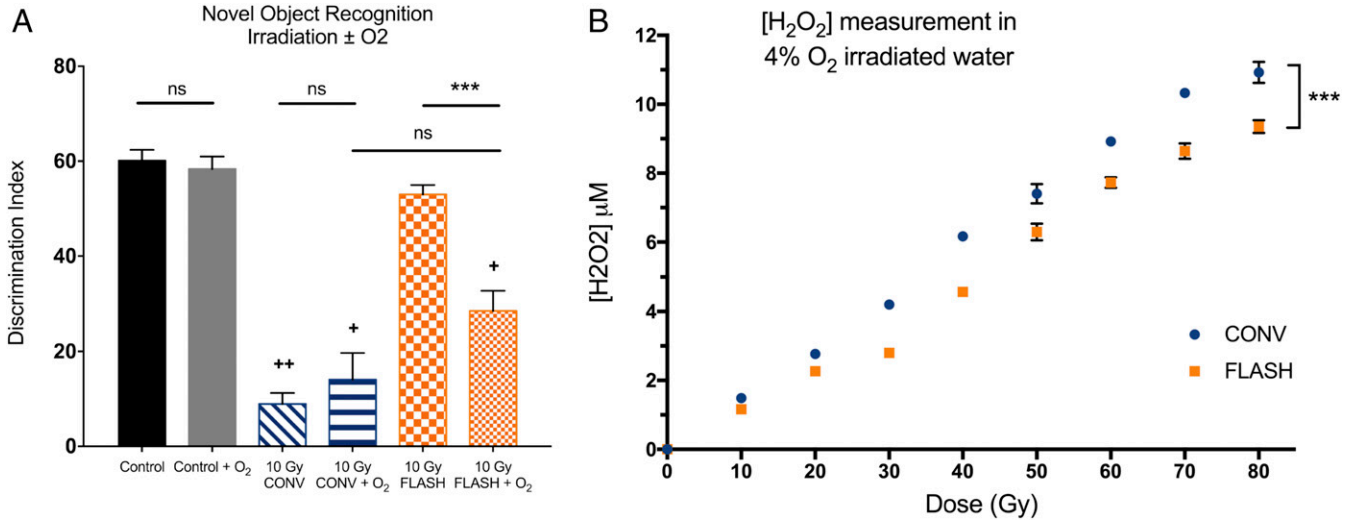

Fig. 2. FLASH effect depends on tissue partial pressure of oxygen (pO_2) and reduced ROS production. WT mice anesthetized under normoxia or carbogen breathing (O_2 groups) were subjected to the NOR test 2 mo postirradiation. (*A*) Increase in normal brain pO_2 caused by carbogen breathing before and during the irradiation delivery reversed the neurocognitive sparing induced by FLASH found under normoxia to levels observed after CONV irradiation. Data are expressed as mean DI ± SD (n = 5–16 animals per group). P values were derived from the Mann–Whitney U test: $^{***}P < 0.001$ compared with the control nonirradiated group and $^{+}P < 0.05$; $^{++}P < 0.01$ compared with the control + O_2 group. ns, not significant. (*B*) Water equilibrated at a 4% O_2 tension was irradiated with CONV and FLASH-RT, and H_2O_2 production was quantified by Amplex Red measurements. FLASH irradiation produces significantly less H_2O_2 than CONV at equivalent doses. Mean ± SD P values were derived from Mann–Whitney U test: $^{***}P < 0.001$.

in the presence of the potent scavengers following FLASH-RT corroborates our hypothesis that FLASH-RT leads to a lower production of ROS, with concomitant reductions in radiation-induced normal tissue damage.

Attenuation of Neuroinflammation by FLASH-RT. Evidence pointing to the mechanistic role of lower ROS levels in mediating the FLASH effect suggested that downstream biological pathways known to be responsive to oxidative injury might be involved. Therefore, given the causal relationship between radiation-induced oxidative stress and inflammation, studies were initiated to investigate the impact of FLASH-RT on neuroinflammatory processes. To start, the expression of GFAP in the striatum of nonirradiated and irradiated mice was quantified by immunofluorescence to assess the occurrence of radiation-induced astrogliosis. No difference between the groups was observed at acute (3-d) times post-RT. However, at 14 d and 2 mo post-RT, the 10-Gy CONV–irradiated group exhibited a significant 3.6-fold and 2.6-fold increase in GFAP immunoreactivity (P = 0.0077 and P = 0.0034, respectively; Fig. 3 *A* and *B*). At 14 d, GFAP staining was located around $CD31^+$ cells, with the presence of numerous astrocytes in close proximity to blood vessels (Fig. 3*A*). At 2 mo, GFAP staining was consistent with the occurrence of radiation-induced scar astrogliosis (Fig. 3*B*). In contrast, the 10-Gy FLASH–irradiated group showed no change in GFAP levels at 14 d and 2 mo post-RT, when cellular staining and localization were similar to those found in the nonirradiated controls (Fig. 3 *A* and *B*). These data indicate that FLASH-RT did not induce subacute activation of astrogliosis or delayed radiation-induced scar astrogliosis, evidence demonstrating the long-lasting benefits of FLASH-RT that might underlie the preservation of cognitive function.

To ascertain the impact of each irradiation modality on microglia, we quantified the number of $IBA\text{-}1^+$ (resting or total) and $CD68^+$ (activated) microglia in the hippocampus at 1 mo and 6 mo after exposure. While resting microglia levels were unresponsive to radiation dose rate (*SI Appendix*, Fig. S3), the response of activated microglia was found to be significantly different in the hippocampus 1 mo following each irradiation modality (Fig. 3*C*). Consistent with past results, CONV irradiation caused a significant increase in the number of $CD68^+$ cells compared with controls ($P < 0.0001$) and, importantly, FLASH irradiation reduced significantly ($P < 0.0001$) the yield of activated microglia to control levels (Fig. 3*D*). Remarkably, similar protective effects were found to persist 6 mo following irradiation (Fig. 3*D*). These data suggest that one mechanism by which FLASH-RT does not cause neurocognitive decline is by reducing radiation-induced ROS, that prevents the early activation of microglia, thereby limiting their transition to a chronically activated state.

Preservation of Host Neuronal Structure and Synaptic Protein Levels by FLASH-RT. Microglia have been shown to actively reshape the synaptic landscape, by pruning dendritic arbors in response to various stressors and microenvironmental cues. Irradiation has also been shown to elicit significant structural plasticity in the irradiated brain, which is able to compromise the morphology of multiple mature neuronal subtypes throughout various regions of the brain (22). Therefore, to determine whether FLASH-RT had a differential impact on neuronal morphology compared with CONV irradiation, mice were analyzed for structural changes in hippocampal granule cell neurons 1 mo and 6 mo after exposure. Reconstructed images revealed a significant loss of dendritic complexity, coupled with a reduction in the number of dendritic spines in the CONV cohort compared with controls 1 mo after exposure, an effect that was not evident in the FLASH-irradiated group (Fig. 4 *A* and *B*). Quantification and analyses of dendritic parameters indicated that FLASH-irradiated cohorts did not exhibit the same level of dendritic alterations in the area ($P < 0.01$), length ($P < 0.05$), and branches ($P < 0.01$) compared with the CONV cohorts (Fig. 4*C*). Further analyses of dendritic spines revealed that compared with CONV cohorts, FLASH-irradiated animals had significantly higher numbers of dendritic spines ($P < 0.05$), elevated spine density ($P < 0.0001$), and higher spine volume ($P < 0.01$) (Fig. 4*D*).

Importantly, long-term analyses were conducted 6 mo following exposure to determine the persistence of any structural changes caused by either irradiation modality. Quantification

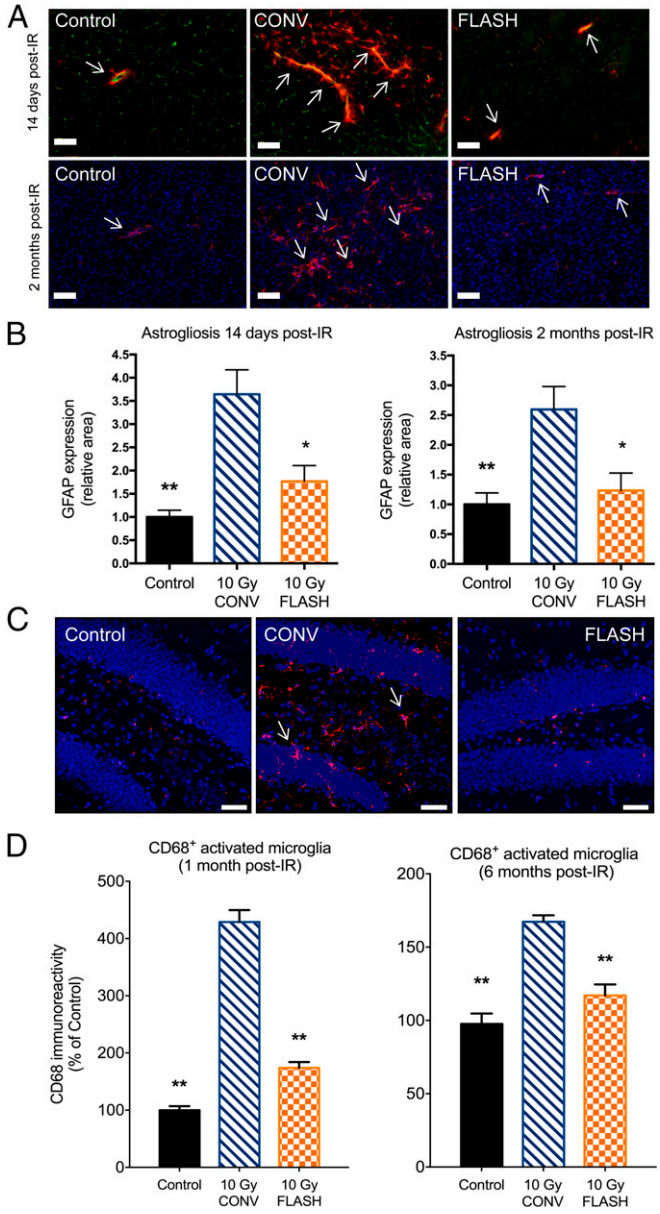

Fig. 3. FLASH-RT reduces indications of neuroinflammation. Micrographs show GFAP$^+$ astrocytes (red) in the vicinity (arrows) of CD31$^+$ endothelial cells (green). (Scale bars: 100 μm.) (*A*) CONV irradiation (IR) leads to a marked rise in GFAP$^+$ cells, indicating an increase in reactive gliosis. FLASH did not elicit such increased levels of reactive gliosis and was comparable to controls. (*B*) Quantification of these data at 2 wk and 2 mo post-IR reveals qualitatively similar yet significant effects. For each post-IR time, CONV IR increased reactive gliosis significantly, whereas FLASH-RT did not, being statistically similar to controls. Mean ± SD (n = 5 animals per group), P values were derived from the nonparametric Mann–Whitney U test: *$P < 0.05$, **$P < 0.01$ compared with the 10-Gy CONV group. (*C*) Micrographs from the hippocampal dentate hilus (DH) and granule cell layer (GCL) show CD68$^+$ activated microglia (red, arrows) against granule cell neurons (blue). (Scale bars: 40 μm.) (*D*) There was a marked increase in activated microglia (CD68$^+$) at both 1 and 6 mo following CONV IR compared with controls. FLASH-RT prevented the increase in activated microglia and was statistically indistinguishable from controls. Mean ± SEM (n = 4 animals per group). P values were derived from ANOVA and the Bonferroni test: **$P < 0.01$ compared with the 10-Gy CONV group.

and analyses of dendritic parameters at this protracted end point revealed that CONV irradiation caused persistent and significant reductions in dendritic area ($P < 0.0001$), length ($P < 0.0001$), and branches ($P < 0.01$) compared with controls. These effects were not found in the FLASH-irradiated cohorts, and compared with CONV cohorts, FLASH irradiation spared significantly dendritic area ($P < 0.0001$), length ($P < 0.0001$), and branches (Fig. 4*E*). Additional analyses of dendritic spine parameters revealed the persistent benefits of FLASH irradiation. At this chronic post-irradiation time point, cohorts subjected to CONV irradiation exhibited significant reductions in dendritic spine density ($P < 0.001$) and volume ($P < 0.0005$), with trends for reduced spine numbers (Fig. 4*F*). While positive trends were found for increased spine numbers after FLASH-RT, multiple comparison analyses indicated that FLASH cohorts exhibited significant increases in spine density ($P < 0.001$) and volume ($P < 0.005$) compared with CONV cohorts (Fig. 4*F*). Morphologic data collected over a 6-mo interval point to the neuroprotective properties of FLASH-RT and provide conclusive evidence that FLASH irradiation does not cause the short- or long-term structural deterioration of mature neuronal morphology that is likely to have an adverse functional impact on cognition.

To investigate further the mechanisms by which FLASH-RT might differentially impact the synaptic landscape in the brain compared with CONV irradiation, we analyzed postsynaptic density protein 95 (PSD-95). Past work has shown CONV irradiation to alter the expression of PSD-95 foci in certain hippocampal and cortical regions of the brain (12, 22), and the current study sought to determine the response of this critical synaptic protein to FLASH irradiation. Interestingly, data indicate that FLASH-RT maintained a synaptic landscape more similar to a nonirradiated brain (*SI Appendix*, Fig. S4).

Discussion

The relative absence of normal tissue toxicity following FLASH irradiation, also known as the "FLASH effect," has caught the field by surprise, representing a rather unexpected outcome. Data presented provide compelling evidence that the FLASH effect is, at least in part, mediated by a lower production of ROS. Thus, FLASH may be able to disrupt and bypass ROS-mediated pathogenic cascades that normally lead to neurocognitive complications and associated pathology typically found after CONV irradiation of the brain. The absence of normal tissue toxicity observed after FLASH irradiation and reported here corroborates recent and older work from our laboratories and others on the normal brain, lung, skin, and gut (18, 19, 23, 24) and, as recently reviewed (25), point to the general applicability of FLASH irradiation to avoid normal tissue injury. Normal tissue sparing reported here is especially relevant in the context of current treatment regimens for adult and pediatric brain tumors that elicit significant toxicities that negatively impact patient care and quality of life (5, 26). Since this unfortunate reality remains an unmet medical need, we used tumor-free animals to investigate the short- and long-term neuroprotective mechanisms of FLASH-RT in the absence of confounding disease.

The comprehensive array of behavioral testing provided compelling evidence that unlike CONV irradiation (27, 28), FLASH-RT did not cause hippocampal- and/or cortical-based deficits in learning and memory and did not result in behaviors characteristic of anxiety and depression. To investigate the potential neuroprotective mechanisms, we explored the role of oxygen and ROS using a series of different model systems and approaches. First, oxygen supplementation (doubling of partial pressure of oxygen) via carbogen breathing (29) in mice was found to reverse the beneficial effects of FLASH on cognition. Follow-up radiochemical studies substantiated that FLASH reduced hydrogen peroxide levels, and in vitro studies found that FLASH could improve clonogenic survival at doses sufficient to adequately deplete oxygen. Scavenging studies implementing millimolar concentrations of antioxidants were then shown to have little to no effect on FLASH-irradiated zebrafish embryos. The foregoing data support the ROS dependence of the FLASH

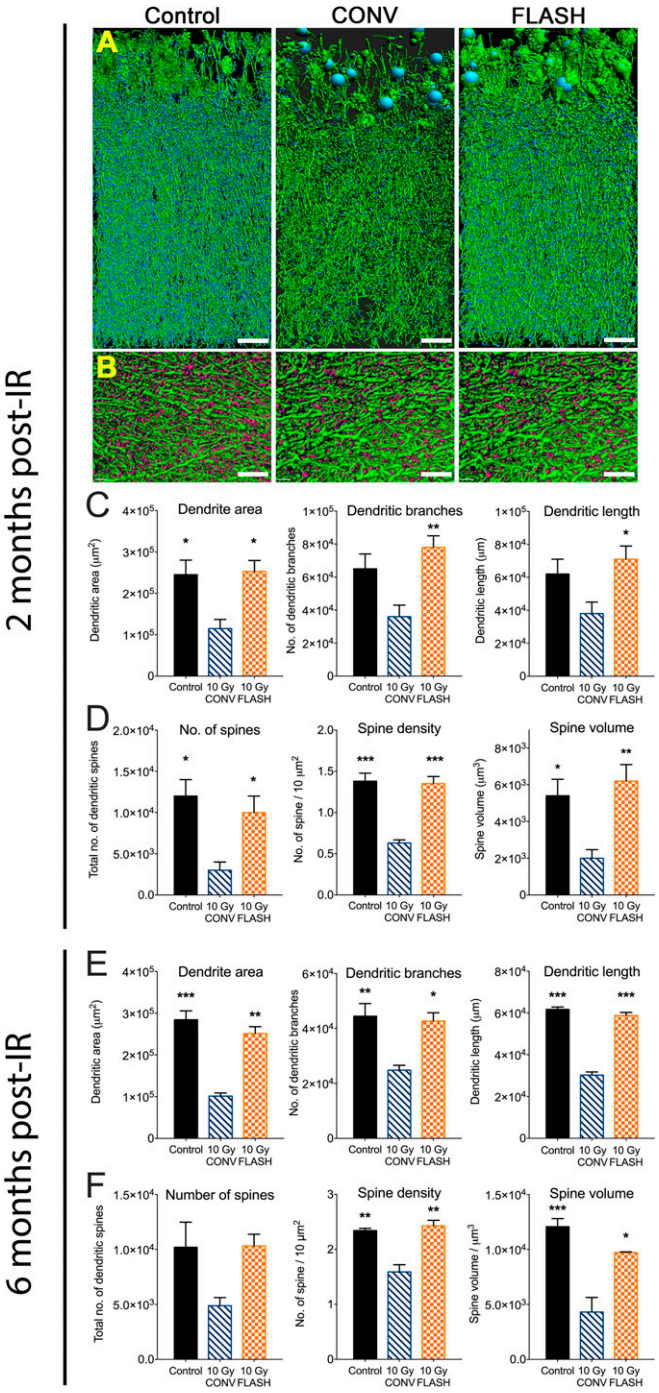

Fig. 4. FLASH-RT preserves host neuronal morphology 2 and 6 mo post-irradiation (post-IR). (*A*) Neuronal dendrites (green) along with major branch points (blue) are shown in each IR cohort. The neuronal arborization is reduced 1 mo post-IR by CONV IR (10-Gy CONV) compared with controls, an effect not apparent after FLASH. (*B*) Higher magnification view of dendritic spines (red) against the dendritic tree (green). Dendritic spine numbers are reduced following CONV IR compared with controls, an effect again not evident in the FLASH-irradiated brain. (Scale bars: *A*, 20 μm; *B*, 5 μm.) (*C*) Reductions in dendritic area, length, and branching following CONV IR compared with controls were evident, effects that were all significantly preserved in the FLASH-irradiated brain. (*D*) Similar findings were evident following quantification of dendritic spines, where reductions in spine numbers, density, and volume were found after CONV IR compared with controls. (*E*) Analyses of granule cell neurons at 6 mo post-IR reveals persistent reductions in dendritic area, length, and branching following CONV IR compared with controls, effects that were all ameliorated significantly in the FLASH-irradiated brain. (*F*) Similar findings were again evident following quantification of dendritic spines, where reductions in spine numbers, density, and volume were found after CONV IR compared with controls. With the exception of spine numbers, FLASH again preserved dendritic spine parameters significantly. Data are expressed as mean ± SEM ($n = 4$ animals per group). *P* values were derived from one-way ANOVA followed by Bonferroni multiple comparison post hoc analysis: $*P < 0.05$, $**P < 0.01$, $***P < 0.001$.

effect, where its cytotoxicity seems dependent primarily on the direct effect. This distinguishes the FLASH effect from CONV irradiation, where both the indirect and direct effects of ionizing radiation govern radiation sensitivity (30).

Our observations are consistent with previous studies showing that bacteria at a given oxygen tension were less sensitive to ultra-high versus CONV irradiation (31, 32). Related results were also obtained with mammalian clonogenic survival (21, 33, 34). Each of these studies concluded that irradiation at an ultra-high dose rate could induce a protective effect via transient depletion of oxygen, but none ever demonstrated the effect in vivo. Although direct oxygen measurement during FLASH irradiation is not feasible in vivo due to the very short time of irradiation (microsecond range), we demonstrate a consistent decrease in ROS production in various systems ranging from a cell-free system to in vitro and complex in vivo models (mouse and zebrafish). We posit that the "instantaneous" depletion of oxygen, and subsequent low level of ROS triggered by FLASH, constitutes one of the primary mechanisms able to modify the entire biological cascade driving normal tissue toxicity.

To support further the role of oxidative stress in the FLASH effect, we investigated the response of oxidative-sensitive pathways in the brain. We explored whether FLASH irradiation might exploit alternative damage surveillance pathways in normal tissue, possibly operating under damage detection thresholds. Interestingly, reactive gliosis and astrogliosis, known to perpetuate neuroinflammatory cascades and vasculature damage and to disrupt CNS functionality in the conventionally irradiated brain (35, 36), were virtually nonexistent in the FLASH-irradiated brain. The conspicuous absence of short- or long-term astrocytic and/or microglial activation was also coincident with a preservation of mature neuronal structure. Of particular significance was the structural preservation of neuronal morphology found 6 mo after FLASH, which included a stabilization of the critical synaptic protein PSD-95 (37, 38). Interestingly, improved cognition (39), reductions in neuroinflammation (40), and protection of dendritic complexity (9) after irradiation have only been documented following stem cell and stem cell-derived exosome transplantation. While these interventions likely operate through trophic support mechanisms, FLASH-RT will most likely operate through completely different mechanisms able to preserve neurotransmission.

Recent and current data make a compelling case for the FLASH technology being at the cusp of changing radiotherapeutic protocols worldwide. Noteworthy too is the surprising realization that FLASH achieves such marked and persistent normal tissue sparing while transpiring within microseconds. Interventions within this rapid timeframe are simply not obtainable from the vast majority of efforts focused on biological and pharmacological strategies, typically able to intervene on processes operating on relative timescales six orders of magnitude slower (Fig. 5*A*). This highlights why this technology stands to change the landscape of radiotherapy, in addition to its obvious capability to freeze organ/tumor motion. Importantly, normal tissues and tumors exhibit differential responses to FLASH (18, 41, 42). This can be rationalized, in part, since normal tissue is already maximally sensitized to ionizing radiation under normoxic conditions (oxygen levels of ~4–6%) and only becomes meaningfully resistant

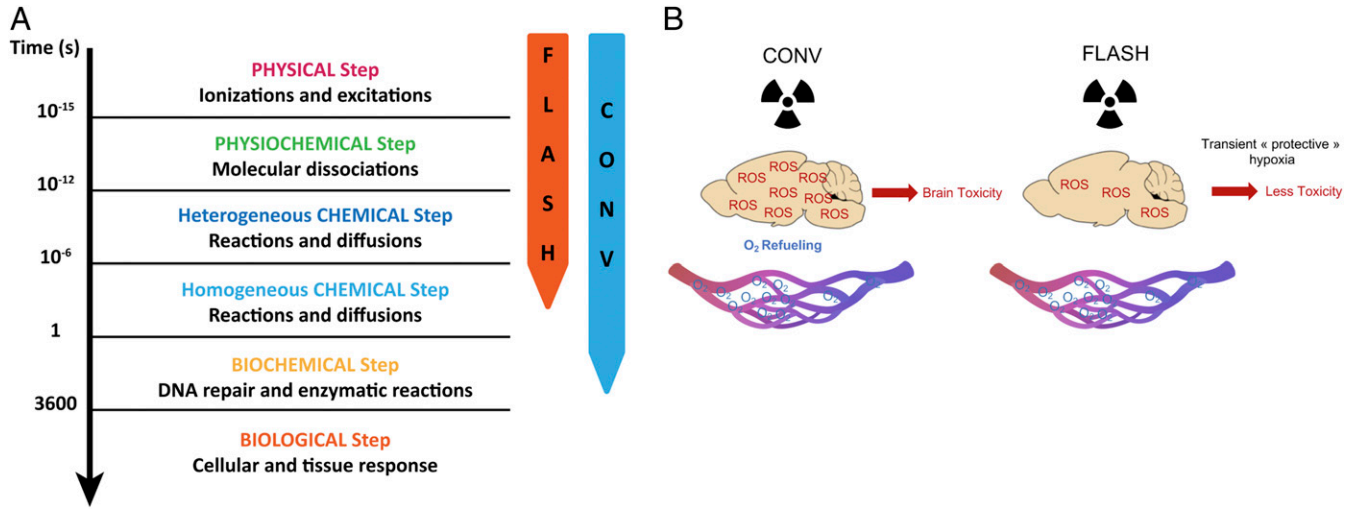

Fig. 5. Differential physicochemical events distinguish FLASH from CONV irradiation. For the delivery of a similar dose, FLASH irradiation is 1,000-fold more rapid than CONV irradiation. (*A*) While CONV irradiation transpires during ongoing chemical and biological responses, FLASH does not interact with these early radiation reactions. (*B*) FLASH induces the rapid depletion of oxygen and a transient local hypoxia, thereby reducing ROS levels and normal brain toxicity compared with CONV irradiation.

under conditions where oxygen levels approach ≤1.5%, whereas tumors, including GBM, contain regions of hypoxia. Lastly, we provide mechanistic evidence that the benefits of FLASH-RT involve reduced production of toxic ROS (Fig. 5*B*). The resultant increase in normal tissue tolerance affords a significant potential for dose escalation, while avoiding severe late effects and toxicities associated with previous chemical modifiers and/or altered fractionation protocols. Further experimentation is clearly needed to fully characterize the biological parameters altered after tissue exposure to FLASH-RT, thereby opening an area of research. However, based on current results, rapid implementation of this promising cancer treatment seems just a matter of time once this technology becomes widely available.

Material and Methods

Irradiation Devices. Irradiation was performed using a prototype 6MeV electron beam linear accelerator (LINAC) of type Oriatron 6e (eRT6; PMB-Alcen), available at Lausanne University Hospital and described previously (43). Physical dosimetry has been extensively described and published to ensure reproducible and reliable biological studies (19, 43–45). This LINAC is able to produce pulsed electron beams at a mean dose rate ranging from 0.1 $Gy{\cdot}s^{-1}$ (i.e., comparable to conventional dose rates used in RT) up to 1,000 $Gy{\cdot}s^{-1}$, corresponding to a dose, in each electron pulse, ranging from 0.01 up to 10 Gy. All FLASH irradiations were performed at a mean dose rate above 100 $Gy{\cdot}s^{-1}$ and at a dose rate within the pulse above $1.8.10^6$ $Gy{\cdot}s^{-1}$. The beam parameters used throughout this study are included in *SI Appendix*, Tables S1–S4. The irradiation settings corresponding to the prescription dose for mouse irradiations were determined by surface dose measurements on a 30 × 30-cm^2 solid water slab positioned behind a 1.7-cm-diameter aperture of a graphite applicator (13.0 × 13.0 × 2.5 cm^3), as previously described (19). The irradiation settings corresponding to the prescription dose for in vitro and zebrafish embryo irradiations were performed in a T41023 water tank (PTW-Freiburg GmbH) with an Advanced Markus ionization chamber (PTW-Freiburg GmbH) corrected for the drop in ion collection efficiency with increased dose per pulse (46).

Animal Experiments. Animal experiments were approved by the Swiss (Vaud state approval: VD2920 and 3241) and University of California, Irvine (Institutional Animal Care and Use Committee) ethics committees for animal experimentation and performed within institutional guidelines.

WBIs. Female C57Bl6/J mice (n = 5–16 animals per group) were purchased from Charles River Laboratories at the age of 8 wk. Tumor-free transgenic mice [n = 10–12 animals per group; strain Tg(*Thy1-eGFP*) MJrsJ, stock no. 007788; The Jackson Laboratory] were bred at the University of California, Irvine animal facility. WBIs were performed under isoflurane anesthesia. The mouse head was positioned behind and in contact with the aperture of the 1.7-cm-diameter graphite applicator to irradiate the whole encephalon region, while limiting the dose to the eyes, the mouth, and the rest of the body. For irradiations in hyperoxic conditions, mice were anesthetized with isoflurane and carbogen (95% O_2, 5% CO_2) for 20 min, including the irradiation time.

Cognitive Testing. To determine the effects of CONV and FLASH irradiations on cognitive function, mice were subjected to behavioral testing 1 and 6 mo after irradiation. Early testing (1 mo) was conducted over 2 wk and included three open-field, spontaneous exploration tasks following our previously described protocols (10, 19, 35, 47). Data analysis was conducted independently and blindly, and is presented as the average of all trials scored for each task. Tumor-free Thy1-EGFP mice were subjected to an extensive neurocognitive test battery to eliminate any confounding effects of disease. These animals were first administered the NOR task, followed by the OIP task and, lastly, the TO task.

The NOR task involved a sequence of habituation (no objects), familiarization (two distinct objects), and, lastly, a test phase in which one of the prior objects is switched with a new one. Animals have a tendency to explore the novel object, and successful performance on this task is reliant on intact perirhinal cortex function (48, 49).

For the OIP task, animals were habituated and then familiarized with four different objects at discrete locations. Following familiarization, the location of two objects is switched and animals are reintroduced to the arena for the test phase and their ability to discriminate the novel object locations. Performance on the OIP task is dependent on intact hippocampal function in addition to the prefrontal and perirhinal cortices (48, 49).

For the TO task, animals were familiarized with two sets of objects 4 h apart. In this instance, mice with functional connectivity between the hippocampus, medial prefrontal cortex (mPFC), and perirhinal cortex show a preference for exploring the prior object, rather than the more recent object (48, 49).

Time spent exploring both familiar and novel objects was counted when the nose of the mouse was within 1 cm and pointed in the direction of the object. Mice did not show object climbing or neophobic behavior. NOR, OIP, and TO data are presented as a DI and calculated as ([Novel location exploration time/Total exploration time] − [Familiar location exploration time/Total exploration time]). A positive index indicates that a mouse spent more time exploring novelty (i.e., switched objects or locations), while a negative score indicates little or no preference for exploring novelty.

Longer term (6 mo) assessments of behavior necessitated the use of tumor-free mice and were designed to assess potential radiation-induced changes in anxiety, depression, and extinction (5, 6, 8, 50–53). The EPM, LDB, and FST tests provide indirect measures of anxiety- and depression-like behavior,

respectively (10, 47). The former two tasks measure an animal's confidence for exploring the open rather than closed arms of a maze or the tendency to move between dark and light areas, while the latter task provides a measure of despair, as animals suffering from depression tend to float more often. These tasks are quantified by calculating the amount of time spent in the open versus closed arms of the EPM, the number of transitions between light and dark regions of the LDB, or the amount of time floating versus swimming during the FST, behaviors that can each be linked to the amygdala (among other regions).

Fear extinction follows a modified fear conditioning protocol (54) in which repeated trials dissociating the tone-shock pairing can be used to measure the rate of reduced freezing or fear extinction. Deficits in this behavior have been linked to the infralimbic region of the mPFC and require active learning, thereby providing a measure of cognitive flexibility. Briefly, mice received three conditioning trials (tone-foot shock pairings) to establish fear. Mice were placed in a conditioning chamber with Plexiglas walls and a metal grid bottom. They were left to acclimate for 2 min and were given the tone followed by a mild foot shock (1 s, 0.7-mA constant current). Freezing was used to measure the conditional fear response during the fear conditioning phase, extinction training phase, and testing phase. At 24 h following conditioning, animals were trained to "unlearn" the association by repeatedly playing the tone without the shock. Mice were given a total of 12 extinction trials (tone alone) in 3 d (3 × 4 trials) to test their ability to extinguish conditioned fear in the same context. The inability to unlearn the association reinforced during conditioning with the tone-foot shock pairing during the extinction and test phases indicates impairment in extinction memory. Deficits in this behavior have been linked to the infralimbic region of the mPFC and require active unlearning, thereby providing another measure of cognitive flexibility, or the ability to adapt to a changing environment (10, 47, 55, 56).

H_2O_2 Production Measurements (Amplex Red). H_2O_2 production measurements were performed using Amplex Red staining. Ultra-pure MilliQ water ($6.9 < pH < 7.1$; 21–22 °C) was equilibrated in a hypoxia hood for 24 h at 4% O_2. Water was irradiated in airtight Eppendorf polypropylene tubes at 0, 10, 20, 30, 40, 50, 60, 70, or 80 Gy at FLASH or CONV in a water tank. AmplexRed was added to the irradiated water (vol/vol) exactly 195 s after the beginning of irradiation at a final concentration of 16.67 μM (previously defined as optimal) and incubated for 90 min protected from light. H_2O_2 solutions from 0.007 to 10 μM were used as standards. Fluorescence quantification was performed using a plate reader 90 min postirradiation (excitation: 530 nm, emission: 590 nm). Measurements were realized in triplicate.

Clonogenic Assays. The isolation and characterization of the murine glioblastoma H454 cells have been described (57). Cells were cultured in DMEM + 10% FBS (Thermo Fisher Scientific) at 37 °C and under different dioxygen concentrations: 4% or 21%. On the day of irradiation, cells were harvested with trypsin + 0.25% EDTA (Thermo Fisher Scientific), counted, and placed in airtight Eppendorf tubes for cell suspension irradiations. Tubes were irradiated in a water tank at 0, 10, or 20 Gy at FLASH or CONV. Cells were then plated at a concentration of 1,000–100,000 cells in six-well plates or Petri dishes and incubated at 37 °C in 5% CO_2, 21% O_2. At 7 d postirradiation, colonies were fixed and stained using Crystal Violet (Sigma). Colonies over 50 cells were counted, and plating efficiency and survival fractions were determined.

Oxidative Stress Measurement in Zebrafish. For in vivo oxidative stress studies, wild-type (WT) zebrafish were bred in our fish facility (Lausanne University Hospital). All in vivo experiments on zebrafish were performed on embryos under 5 dpf. Fertilized WT zebrafish eggs were incubated at 28 °C until 5 dpf. Anesthesia was performed with 168 mg/L tricaine, and 10–20 embryos were transferred in 2-mL Eppendorf tubes. Water + tricaine was then removed and replaced by pure H_2O + 60 mg/L ocean salt. For antioxidant treatments on WT animals, NAC (5 mM, pH 7.5; Sigma) or amifostine (4 mM; Sigma–Aldrich) was added to the water 1 h before irradiation. Irradiation was performed 4 hpf at 8-Gy FLASH and CONV in 2-mL Eppendorf tubes placed in a water tank as described above. Embryos were fixed 5 dpf with a solution of paraformaldehyde (4% final concentration) before microscopic analysis (Evos XL Core Cell Imaging System; Thermo Fisher Scientific). Fish length was measured using ImageJ 1.X. software.

Immunohistochemistry, Confocal Microscopy, and Quantification. At select times postirradiation, animals were prepared for immunohistochemistry as described previously (9). Brains were cryoprotected (30% sucrose) and sectioned coronally (30–35 μm thick) using a cryostat (Leica Microsystems). For astrogliosis, GFAP and CD31 expression was assessed in the striatum of control and irradiated mice. Floating brain sections were incubated with anti-GFAP (1:500; clone GA5; MAB360) and anti-CD31 (1:150, 553370; BD Biosciences) primary antibodies. Alexa Fluor 568-labeled goat anti-mouse (1:200, A21124; Thermo Fisher Scientific) and Alexa 488-labeled donkey anti-rat (1:200, A11070; Thermo Fisher Scientific) secondary antibodies were used. Two to four sections per animal were mounted on microscope slides with Vectashield + DAPI (H-1500; Vector Laboratories). Image acquisition was performed using an upright Zeiss Axiovison microscope. GFAP expression area was quantified using ImageJ software.

For the assessment of microglia, the following primary and secondary antibodies were used: rabbit anti–IBA-1 (1:500; Wako), rat anti-mouse CD68 (1:500; AbD Serotec), donkey anti-rabbit or anti-mouse conjugated with Alexa Fluor 488 or 594 (Life Technologies/Invitrogen), and DAPI nuclear counterstain (Sigma–Aldrich). Representative sections (three to four sections per animal, four to six animals per group) through the middle of the hippocampus were selected, and immunofluorescence staining followed procedures described in detail previously (16, 58). Immunofluorescent sections were imaged using a Nikon Eclipse Ti C2 microscope to obtain 20–30 Z-stacks (1,024 × 1,024 pixels, 1 μm each) using 10× and 60× PlanApo oil-immersion lens (Nikon). For quantification of IBA-1^+ and $CD68^+$ cells, 3D deconvolution and reconstruction were carried out using the AutoQuantX3 algorithm (MediaCybernetics). Quantification was facilitated using the Imaris spot tool (v8.0; Bit Plane, Inc.).

The assessment of PSD-95 foci has been described previously (12, 22). Briefly, serial 30-μm-thick sections (three per animal) from the anterior-to-posterior hippocampus were selected, and three different fields in each section were imaged from the dentate gyrus. Images were collected using a Nikon Eclipse TE 2000-U microscope with 0.5-μm-interval high-resolution Z-stacks (1,024 × 1,024 pixels). Analysis of PSD-95 was performed using the Imaris spot tool, and puncta satisfying predefined criteria (verified visually for accuracy) were converted to spots for quantification under preset parameters kept constant throughout subsequent analyses.

Morphometric Assessments of Neurons. Details regarding the reconstruction of neurons and the morphologic classification of spines have been described (12, 22). For dendritic analyses, 100-μm-thick hippocampal sections were prepared for confocal imaging. Three sections per animal were used to generate Z-stacks from four animals using a Nikon Eclipse TE 2000-U microscope. Images comprising each Z-stack (1,024 × 1,024 pixels) were acquired (60×) over the entire dendrite tree at 0.5-μm increments. Quantification of dendritic parameters was derived from Z-stacks reconstructed in three dimensions from deconvoluted images using the AutoQuantX3 algorithm. Deconvoluted 3D reconstructions yielded high spatial resolution images for detailed dendritic tracing and spine classification using the Imaris software suite (Bitplane, Inc.) as described previously (12, 22). For spines to be included in our analyses, a maximum spine length and minimum spine end diameter were set at 2.5 nm and 0.4 nm, respectively. Parameters of neuronal structure that were identified and quantified through image reconstruction and deconvolution using the Imaris software suite included the cell body, dendritic and axonal length, branching and branch points, dendritic complexity, spines, and boutons.

Statistics. Statistical analyses were carried out using GraphPad Prism (v6) software. One-way ANOVA was used to assess significance between control and irradiated groups, and when overall group effects were found to be statistically significant, a Bonferroni multiple comparisons test was used to compare the control and FLASH groups against the CONV cohort. In addition, the unpaired nonparametric Mann–Whitney *U* test or unpaired *t* test after Gaussian distribution assessment by the Shapiro–Wilk normality test were used. Results were expressed as mean values ± SD or mean values ± SEM, and all analyses considered a value of $P \leq 0.05$ to be statistically significant.

ACKNOWLEDGMENTS. We thank the Animal Facilities of Epalinges and University of California, Irvine for animal husbandry; the zebrafish team (F. Amati, Y. Arribat, A. Reymond, and N. Voisin); and A. de Vallière for astrogliosis studies. The study was supported by a grant from the Swiss National Fund (SNF) (31003A_156892, to M.C.V. and J.B.), by a grant from the Fond'action (to J.B.), by a grant from SNF/French National Agency from Research (CR32I3L_156924, to M.C.V.), by the ISREC Foundation thanks to a Biltema donation (to M.C.V. and J.B.), by National Institute of Neurological Disorders and Stroke Grant NS089575 (to C.L.L.), and by KL2 Award KL2TR001416 (to M.M.A.). P.M.-G. was supported by an Ecole Normale Supérieure de Cachan Fellowship (Ministère de l'Enseignement Supérieur et de la Recherche).

1. Begg AC, Stewart FA, Vens C (2011) Strategies to improve radiotherapy with targeted drugs. *Nat Rev Cancer* 11:239–253.
2. Bentzen SM (2006) Preventing or reducing late side effects of radiation therapy: Radiobiology meets molecular pathology. *Nat Rev Cancer* 6:702–713.
3. Yarnold J, Brotons MC (2010) Pathogenetic mechanisms in radiation fibrosis. *Radiother Oncol* 97:149–161.
4. Bortfeld T (2006) IMRT: A review and preview. *Phys Med Biol* 51:R363–R379.
5. Butler JM, Rapp SR, Shaw EG (2006) Managing the cognitive effects of brain tumor radiation therapy. *Curr Treat Options Oncol* 7:517–523.
6. Caceres LG, et al. (2013) Pharmacological alterations that could underlie radiation-induced changes in associative memory and anxiety. *Pharmacol Biochem Behav* 111: 37–43.
7. Meyers CA, Hess KR, Yung WK, Levin VA (2000) Cognitive function as a predictor of survival in patients with recurrent malignant glioma. *J Clin Oncol* 18:646–650.
8. Wellisch DK, Kaleita TA, Freeman D, Cloughesy T, Goldman J (2002) Predicting major depression in brain tumor patients. *Psychooncology* 11:230–238.
9. Baulch JE, et al. (2016) Cranial grafting of stem cell-derived microvesicles improves cognition and reduces neuropathology in the irradiated brain. *Proc Natl Acad Sci USA* 113:4836–4841.
10. Parihar VK, et al. (2016) Cosmic radiation exposure and persistent cognitive dysfunction. *Sci Rep* 6:34774.
11. Parihar VK, et al. (2015) Targeted overexpression of mitochondrial catalase prevents radiation-induced cognitive dysfunction. *Antioxid Redox Signal* 22:78–91.
12. Parihar VK, Limoli CL (2013) Cranial irradiation compromises neuronal architecture in the hippocampus. *Proc Natl Acad Sci USA* 110:12822–12827.
13. Craver BM, et al. (2016) 3D surface analysis of hippocampal microvasculature in the irradiated brain. *Environ Mol Mutagen* 57:341–349.
14. Lee WH, Cho HJ, Sonntag WE, Lee YW (2011) Radiation attenuates physiological angiogenesis by differential expression of VEGF, Ang-1, tie-2 and Ang-2 in rat brain. *Radiat Res* 176:753–760.
15. Warrington JP, et al. (2011) Cerebral microvascular rarefaction induced by whole brain radiation is reversible by systemic hypoxia in mice. *Am J Physiol Heart Circ Physiol* 300:H736–H744.
16. Acharya MM, et al. (2016) Elimination of microglia improves cognitive function following cranial irradiation. *Sci Rep* 6:31545.
17. Moravan MJ, Olschowka JA, Williams JP, O'Banion MK (2011) Cranial irradiation leads to acute and persistent neuroinflammation with delayed increases in T-cell infiltration and CD11c expression in C57BL/6 mouse brain. *Radiat Res* 176:459–473.
18. Favaudon V, et al. (2014) Ultrahigh dose-rate FLASH irradiation increases the differential response between normal and tumor tissue in mice. *Sci Transl Med* 6:245ra93.
19. Montay-Gruel P, et al. (2017) Irradiation in a flash: Unique sparing of memory in mice after whole brain irradiation with dose rates above 100Gy/s. *Radiother Oncol* 124: 365–369.
20. Weiss H, Epp ER, Heslin JM, Ling CC, Santomasso A (1974) Oxygen depletion in cells irradiated at ultra-high dose-rates and at conventional dose-rates. *Int J Radiat Biol Relat Stud Phys Chem Med* 26:17–29.
21. Epp ER, Weiss H, Djordjevic B, Santomasso A (1972) The radiosensitivity of cultured mammalian cells exposed to single high intensity pulses of electrons in various concentrations of oxygen. *Radiat Res* 52:324–332.
22. Parihar VK, et al. (2015) Persistent changes in neuronal structure and synaptic plasticity caused by proton irradiation. *Brain Struct Funct* 220:1161–1171.
23. Loo B, et al. (2017) Delivery of ultra-rapid flash radiation therapy and demonstration of normal tissue sparing after abdominal irradiation of mice. *Int J Radiat Oncol Biol Phys* 98:E16.
24. Vozenin MC, et al. (2019) The advantage of FLASH radiotherapy confirmed in mini-pig and cat-cancer patients. *Clin Cancer Res* 25:35–42.
25. Vozenin M-C, Hendry J, Limoli C (April 19, 2019) Biological benefits of ultra-high dose-rate FLASH radiotherapy: Sleeping beauty awoken. *Clin Oncol (R Coll Radiol)*, 10.1016/j.clon.2019.04.001.
26. Meyers CA (2000) Neurocognitive dysfunction in cancer patients. *Oncology (Williston Park)* 14:75–79; discussion 79, 81–82, 85.
27. Kaplan GB, et al. (2018) Pathophysiological bases of comorbidity: Traumatic brain injury and post-traumatic stress disorder. *J Neurotrauma* 35:210–225.
28. Wessa M, Flor H (2007) Failure of extinction of fear responses in posttraumatic stress disorder: Evidence from second-order conditioning. *Am J Psychiatry* 164:1684–1692.
29. Khan N, et al. (2009) Tissue pO2 of orthotopic 9L and C6 gliomas and tumor-specific response to radiotherapy and hyperoxygenation. *Int J Radiat Oncol Biol Phys* 73: 878–885.
30. Ward JF (1988) DNA damage produced by ionizing radiation in mammalian cells: Identities, mechanisms of formation, and reparability. *Prog Nucleic Acid Res Mol Biol* 35:95–125.
31. Dewey DL (1969) An oxygen-dependent X-ray dose-rate effect in Serratia marcescens. *Radiat Res* 38:467–474.
32. Dewey DL, Boag JW (1959) Modification of the oxygen effect when bacteria are given large pulses of radiation. *Nature* 183:1450–1451.
33. Ling CC, Michaels HB, Epp ER, Peterson EC (1978) Oxygen diffusion into mammalian cells following ultrahigh dose rate irradiation and lifetime estimates of oxygen-sensitive species. *Radiat Res* 76:522–532.
34. Michaels HB, Epp ER, Ling CC, Peterson EC (1978) Oxygen sensitization of CHO cells at ultrahigh dose rates: Prelude to oxygen diffusion studies. *Radiat Res* 76:510–521.
35. Acharya MM, et al. (2016) Adenosine kinase inhibition protects against cranial radiation-induced cognitive dysfunction. *Front Mol Neurosci* 9:42.
36. Liddelow SA, et al. (2017) Neurotoxic reactive astrocytes are induced by activated microglia. *Nature* 541:481–487.
37. Keith D, El-Husseini A (2008) Excitation control: Balancing PSD-95 function at the synapse. *Front Mol Neurosci* 1:4.
38. Preissmann D, et al. (2012) Increased postsynaptic density protein-95 expression in the frontal cortex of aged cognitively impaired rats. *Exp Biol Med (Maywood)* 237:1331–1340.
39. Acharya MM, et al. (2009) Rescue of radiation-induced cognitive impairment through cranial transplantation of human embryonic stem cells. *Proc Natl Acad Sci USA* 106: 19150–19155.
40. Acharya MM, et al. (2015) Defining the optimal window for cranial transplantation of human induced pluripotent stem cell-derived cells to ameliorate radiation-induced cognitive impairment. *Stem Cells Transl Med* 4:74–83.
41. Bourhis J, et al., Clinical translation of FLASH radiotherapy: Why and how? *Radiother Oncol*, in press.
42. Spitz DR, et al. (April 19, 2019) An integrated physico-chemical approach for explaining the differential impact of FLASH versus conventional dose rate irradiation on cancer and normal tissue responses. *Radiother Oncol*, 10.1016/j.radonc.2019.03.028.
43. Jaccard M, et al. (2018) High dose-per-pulse electron beam dosimetry: Commissioning of the Oriatron eRT6 prototype linear accelerator for preclinical use. *Med Phys* 45: 863–874.
44. Jaccard M, et al. (2017) High dose-per-pulse electron beam dosimetry: Usability and dose-rate independence of EBT3 Gafchromic films. *Med Phys* 44:725–735.
45. Petersson K, et al. (2017) High dose-per-pulse electron beam dosimetry–A model to correct for the ion recombination in the Advanced Markus ionization chamber. *Med Phys* 44:1157–1167.
46. Petersson K, et al. (2016) High dose-per-pulse electron beam dosimetry–A saturation model for the Advanced Markus ionization chamber. *Strahlentherapie Und Onkol* 192:848–849.
47. Parihar VK, et al. (2018) Persistent nature of alterations in cognition and neuronal circuit excitability after exposure to simulated cosmic radiation in mice. *Exp Neurol* 305:44–55.
48. Barker GR, Bird F, Alexander V, Warburton EC (2007) Recognition memory for objects, place, and temporal order: A disconnection analysis of the role of the medial prefrontal cortex and perirhinal cortex. *J Neurosci* 27:2948–2957.
49. Barker GR, Warburton EC (2011) When is the hippocampus involved in recognition memory? *J Neurosci* 31:10721–10731.
50. Andersen BL, Tewfik HH (1985) Psychological reactions to radiation therapy: Reconsideration of the adaptive aspects of anxiety. *J Pers Soc Psychol* 48:1024–1032.
51. Kaleita TA, et al. (2006) Pilot study of modafinil for treatment of neurobehavioral dysfunction and fatigue in adult patients with brain tumors. *J Clin Oncol* 24:1503 (abstr).
52. Tang Y, Luo D, Rong X, Shi X, Peng Y (2012) Psychological disorders, cognitive dysfunction and quality of life in nasopharyngeal carcinoma patients with radiation-induced brain injury. *PLoS One* 7:e36529.
53. Yen PN, et al. (2014) Risk factors of depression after prolonged low-dose rate environmental radiation exposure. *Int J Radiat Biol* 90:859–866.
54. Christie LA, et al. (2012) Impaired cognitive function and hippocampal neurogenesis following cancer chemotherapy. *Clin Cancer Res* 18:1954–1965.
55. Milad MR, Quirk GJ (2002) Neurons in medial prefrontal cortex signal memory for fear extinction. *Nature* 420:70–74.
56. Xie C, Han Y, Liu Y, Han L, Liu J (2014) miRNA-124 down-regulates SOX8 expression and suppresses cell proliferation in non-small cell lung cancer. *Int J Clin Exp Pathol* 7: 6534–6542.
57. Shchors K, Massaras A, Hanahan D (2015) Dual targeting of the autophagic regulatory circuitry in gliomas with repurposed drugs elicits cell-lethal autophagy and therapeutic benefit. *Cancer Cell* 28:456–471.
58. Acharya MM, et al. (2015) Consequences of low dose ionizing radiation exposure on the hippocampal microenvironment. *PLoS One* 10:e0128316.

PNAS
www.pnas.org

Supplementary Information for

Long-term neurocognitive benefits of FLASH radiotherapy driven by reduced reactive oxygen species.

Pierre Montay-Gruel[1*], Munjal M. Acharya [2*], Kristoffer Petersson[1, 3], Leila Alikhani[2], Chakradhar Yakkala[1], Barrett D. Allen[2], Jonathan Ollivier[1,4], Benoit Petit[1,4], Patrik Gonçalves Jorge[1, 3], Amber R. Syage[2], Thuan A. Nguyen[2], Al Anoud D. Baddour[2], Celine Lu[2], Paramvir Singh[2], Raphael Moeckli[3], François Bochud[3], Jean-François Germond[3], Pascal Froidevaux[3], Claude Bailat[3], Jean Bourhis[1,4], Marie-Catherine Vozenin[1,4°] and Charles L. Limoli[2°].

Corresponding authors:
Marie-Catherine Vozenin
E-mail: marie-catherine.vozenin@chuv.ch

Charles Limoli
E-mail: climoli@uci.edu

This PDF file includes:

Supplementary Figs. S1 to S4
Supplementary Tables T1 to T4

Supporting Information

Supplemental Figures, Legends and Tables

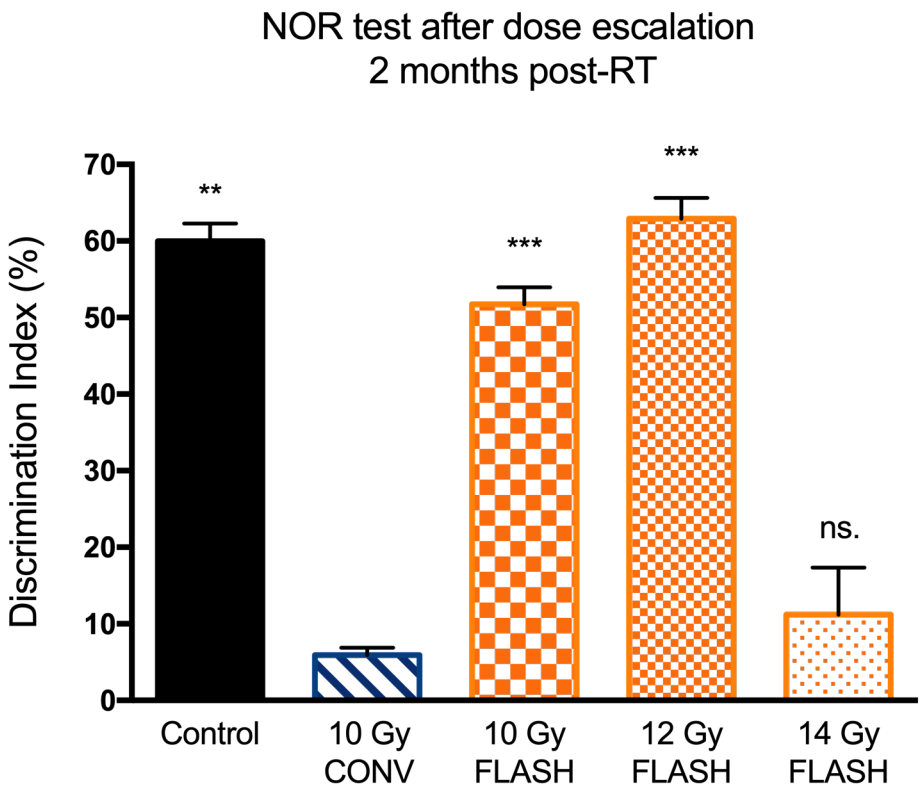

Figure S1: Radiation-induced neurocognitive assessments after dose escalation with FLASH-RT

WT mice were tested using the novel object recognition (NOR) task. Conventional-dose-rate irradiation at 10 Gy caused significant reductions in DI whereas 10 and 12 Gy doses administered by FLASH prevented radiation-induced cognitive deficits. Interestingly, at the higher dose of 14 Gy, the benefits of FLASH were lost, as DI values were similar to that found after conventional dose-rate irradiation. Mean ±SEM (*N*=5-13 mice/group), *P* values derived from unpaired t-tests performed after Gaussian distribution assessment with Shapiro test. ***P*<0.01; ****P*<0.001, compared to the 10 Gy CONV group.

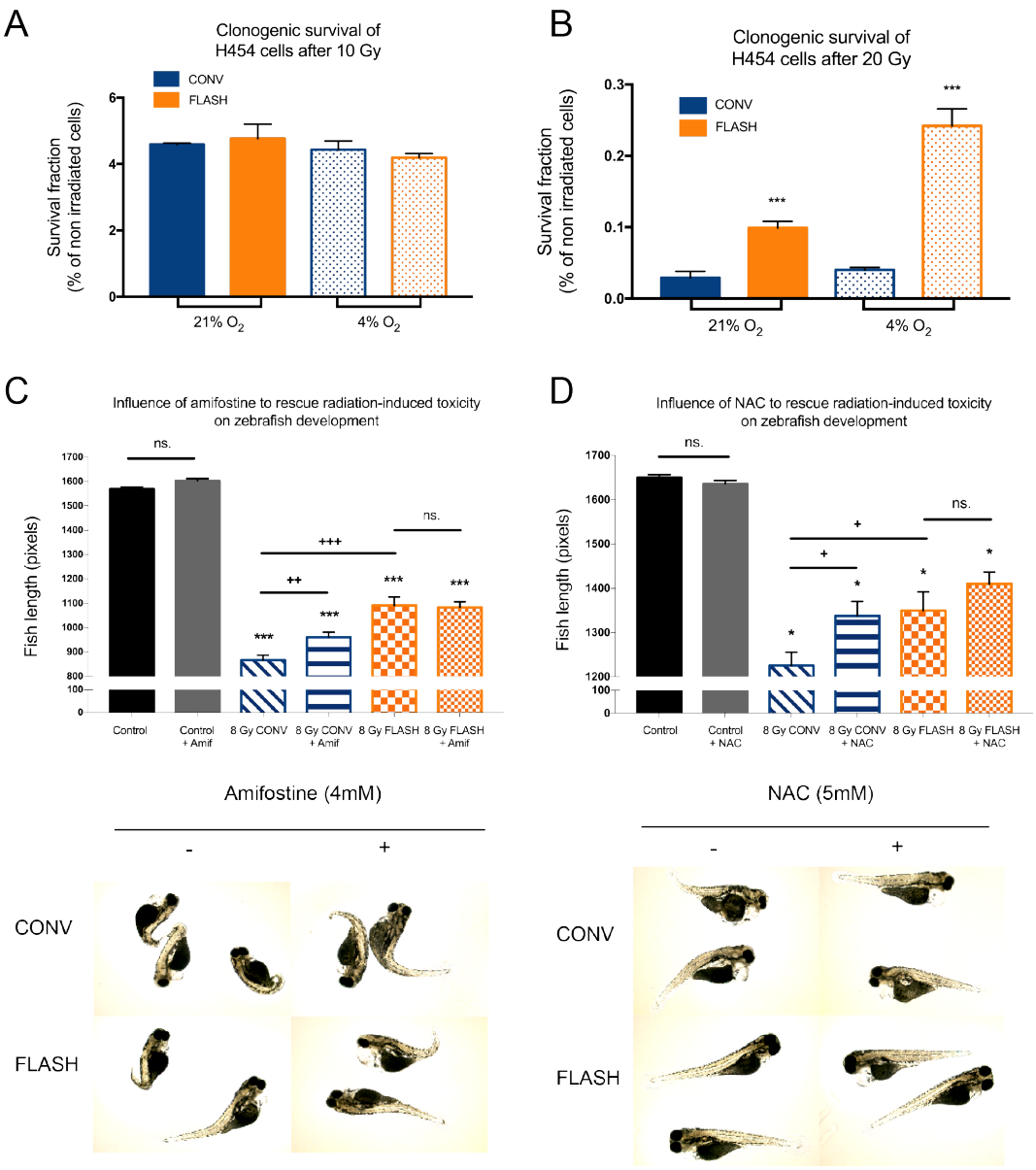

Figure S2: The FLASH effect occurs at high dose and induces oxidative stress
H454 clonogenic survival was quantified after the delivery of 10 (**A**) or 20 Gy (**B**) at CONV or FLASH-RT and under atmospheric (21%) or physiologic (4%) oxic conditions. Clonogenic survival of H454 cells is found to be higher after the delivery of 20 Gy with FLASH-RT and in physiologic oxic conditions (**B**). Mean ± SD. *P* values derived from Mann-Whitney's-test: ***P<0.001 (N=3 assays). Radiation-induced alterations of zebrafish morphology were assessed by body length measurements following 8 Gy in the presence of antioxidants (4mM Amifostine (**C**) or 5mM NAC (**D**). FLASH induced fewer morphological alterations than all other irradiated groups. In contrast to the groups irradiated with conventional irradiation, the treatment with both antioxidants did not ameliorate the radiation-induced toxicity mediated with FLASH. Mean ± SD. *P* values derived from Mann-Whitney's-test: *P<0.05; ** P<0.01; ***P<0.001 (N=9-19 embryos/group).

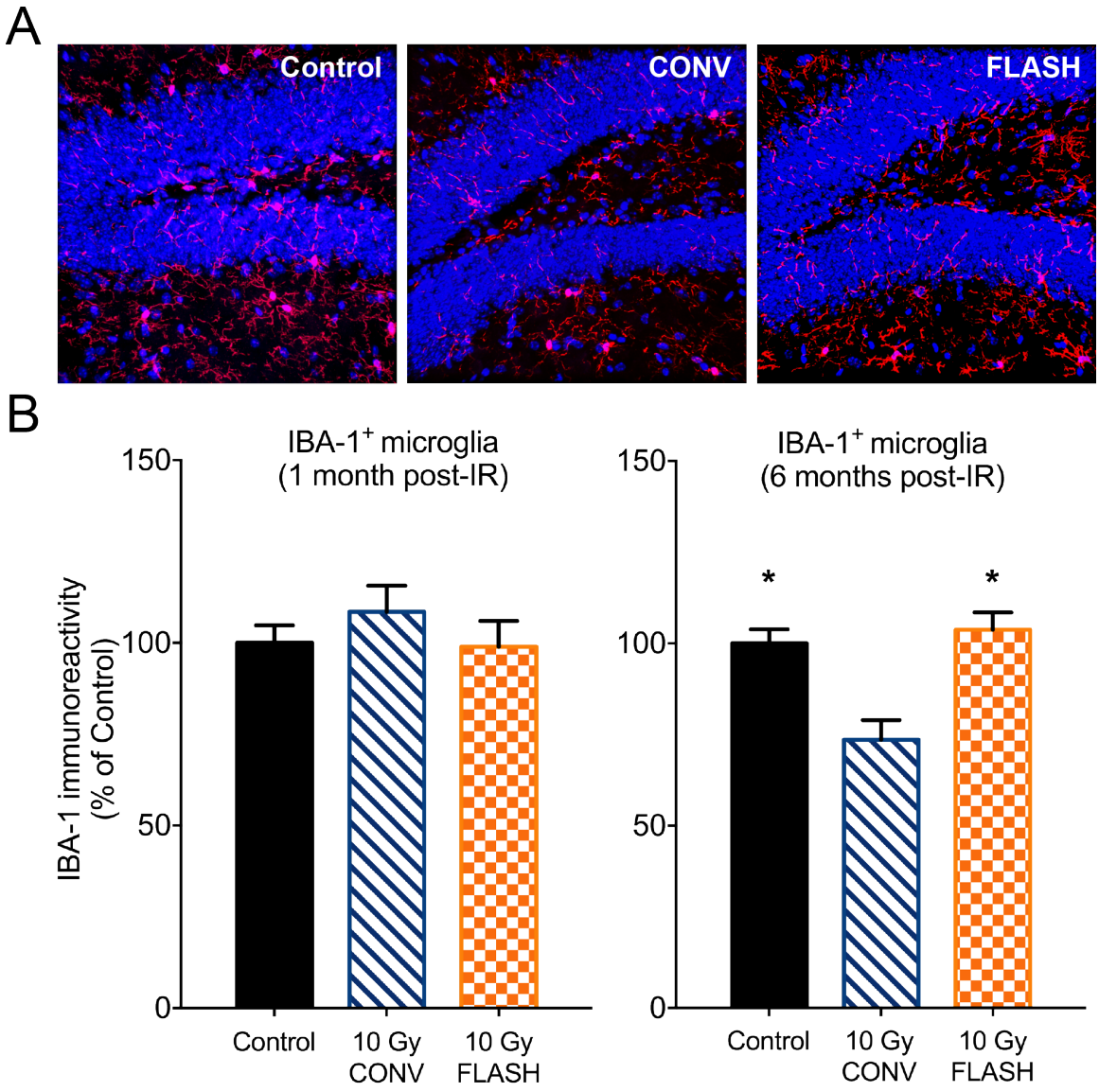

Figure S3: FLASH-RT has a minimal impact on resting microglia. Immunofluorescence staining and laser scanning confocal microcopy was performed on brain sections selected from each irradiated cohort. Representative high-resolution (60×) confocal micrographs from the hippocampal dentate hilus (DH) and granule cell layer (GCL) show IBA-1$^+$ microglial cell bodies (red) against the background of granule cell neurons (blue) for each of the experimental cohorts (**A**). Quantification of IBA-1$^+$ microglia show little effect at 1 month, but a reduction at 6 months after conventional dose-rate irradiation (**B**). For resting microglia, FLASH cohort was statistically indistinguishable from controls at each of these time points (**B**). Data are presented as mean ±SEM (*N*=4animals/group. *P* values derived from ANOVA and Bonferroni's multiple comparisons test. **P*< 0.05; ***P*< 0.01, compared to the 10 Gy CONV group.

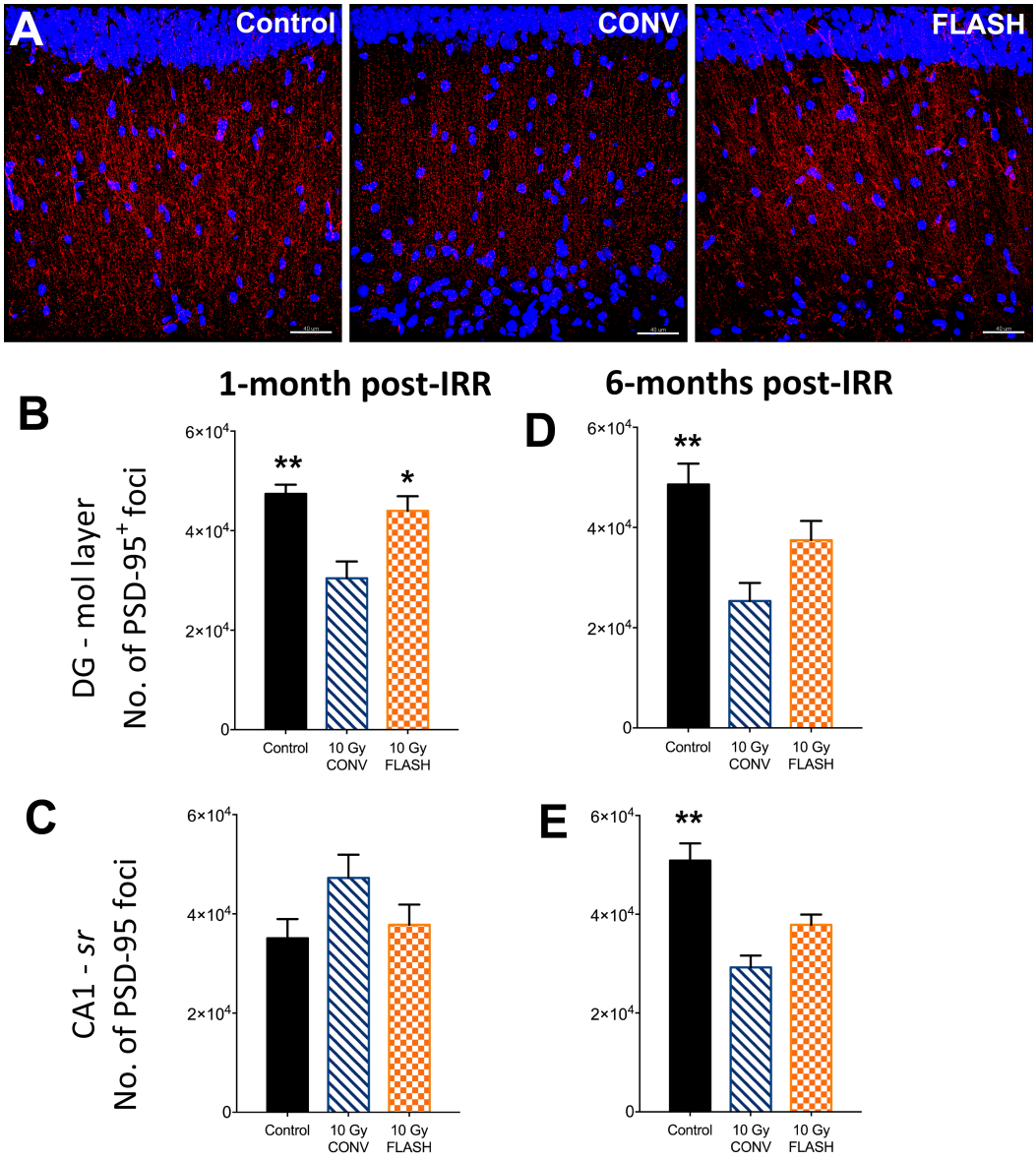

Figure S4: FLASH-RT does not perturb PSD-95 levels compared to conventional dose-rate irradiation.

Representative fluorescence micrographs showing PSD-95 puncta (red) against the soma (blue) of granule cell neurons following each irradiation modality (**A**). Quantitative analyses of fluorescent PSD-95 foci show that exposure to conventional dose-rate reduces PSD-95 levels in the dentate gyrus (DG) at both 1 (**B**) and 6 months (**D**) following exposure compared to controls, an effect not found in the FLASH irradiated brain. Analysis of CA1 pyramidal cell neurons reveals different trends in PSD-95 levels after irradiation, but after 1 month (**C**) or 6 month (**E**), the FLASH irradiated brain was similar to controls, and did not show the types of changes evident after conventional dose-rate irradiation. Data are expressed as the mean ± SEM. *P< 0.05; **P< 0.01; Two-way repeated ANOVA followed by Bonferroni post-hoc test.

Supplementary Table 1

Normal tissue toxicity +/-carbogen (Fig. 1-4 and Fig. S1-S3)		Beam parameters				
Mode	Prescribed Dose (Gy)	Frequency (Hz)	SSD (mm)	Pulse width (μs)	Number of pulses	Treatment time (s)
CONV	10	10	612-800	1.0	639-1180	63.8-117.9
FLASH	10	100	350	1.8	1	$1.8 \cdot 10^{-6}$
	12	100	320	1.8	1	$1.8 \cdot 10^{-6}$
	14	100	297	1.8	1	$1.8 \cdot 10^{-6}$

Supplementary Table 2

Pure water (Fig. 5A)		Beam parameters				
Mode	Prescribed Dose (Gy)	Frequency (Hz)	SSD (mm)	Pulse width (μs)	Number of pulses	Treatment time (s)
CONV	10	10	400	1.0	350	349.9
	20				696	69.5
	30				1047	104.6
	40				1390	138.8
	50				1730	172.9
	60				2075	207.4
	70				2440	243.9
	80				2800	279.9
FLASH	10	100	460	1.75	2	0.01
	20			1.8	4	0.03
	30			1.84	6	0.05
	40			1.87	8	0.07
	50			1.89	10	0.09
	60			1.9	12	0.11
	70			1.87	14	0.13
	80			1.87	16	0.15

Supplementary Table 3

Clonogenic cell survival (Fig. 5B)		Beam parameters				
Mode	Prescribed Dose (Gy)	Frequency (Hz)	SSD (mm)	Pulse width (µs)	Number of pulses	Treatment time (s)
CONV	10	10	400	1.0	505	50.4
	20				1000	99.9
FLASH	10	100	335	1.98	2	0.01
	20		388	1.48	3	0.02

Supplementary Table 4

Fish eggs; +/- NAC +/- Amifostine (Fig. 5C)		Beam parameters				
Mode	Prescribed Dose (Gy)	Frequency (Hz)	SSD (mm)	Pulse width (µs)	Number of pulses	Treatment time (s)
CONV	8	10	808	1.0	1262	126.1
FLASH	8	200	350	1.49	1	$1.49 \cdot 10^{-6}$